Remote Sensing of Environment 208 (2018) 97–108

Contents lists available at ScienceDirect

Remote Sensing of Environment

journal homepage: www.elsevier.com/locate/rse

Observation of sea surface roughness at a pixel scale using multi-angle sun glitter images acquired by the ASTER sensor

Huaguo Zhang[a,*], Kang Yang[a], Xiulin Lou[a], Yan Li[a,b], Gang Zheng[a], Juan Wang[a], Xiaozhen Wang[a], Lin Ren[a], Dongling Li[a], Aiqin Shi[a]

[a] State Key Laboratory of Satellite Ocean Environment Dynamics, Second Institute of Oceanography, State Oceanic Administration, Hangzhou 310012, China
[b] Fujian Provincial Key Laboratory for Coastal Ecology and Environmental Studies, Xiamen University, Xiamen 361005, China

ARTICLE INFO

Keywords:
Sea surface roughness
Mean square slope
Multi-angle sun glitter
Wind speed
ASTER

ABSTRACT

Sea surface roughness (SSR) is commonly used to describe the state of the sea surface. Sun glitter (SG), caused by direct specular reflection of sunlight from the sea surface, and its intensity are strongly affected by SSR. Here, we propose a new model for estimating SSR at a pixel scale using multi-angle SG images. To test our model, high-resolution multi-angle SG images acquired by the Advanced Spaceborne Thermal Emission and Reflection Radiometer (ASTER) sensor were used to estimate SSR. The modal value of SSR was more suitable for describing the background SSR induced by wind, and these data were then converted into wind speed for accuracy evaluation. The estimated wind matched reasonably well with corresponding reanalysis wind data from the European Centre for Medium-Range Weather Forecasting and buoy wind data from the National Data Buoy Center. The results showed that the proposed model has an inversion accuracy that is comparable to other remote sensing methods. Next, we presented three examples of high-resolution SSR images of an oil slick, submarine topography, and internal wave information to illustrate the applications of the model. These estimated SSR images showed detailed oceanographic features with low noise and quantitative changes in SSR at a pixel scale. The results of this study demonstrate that it is feasible to estimate SSR at a high resolution using multi-angle SG images, and high-resolution SSR observations have considerable applicability to oceanographic phenomena.

1. Introduction

Waves are distinguishing features of the sea surface that can be primarily described by sea surface roughness (SSR) (Drennan et al., 2005). Gravity-capillary waves, which encompass centimetric length waves mainly induced by local wind stress, are a dominant part of the wave spectrum used for describing SSR. Sea surface roughness is a key physical parameter in studies of air–sea interactions and ocean dynamics. However, it is difficult to measure SSR directly because of the complexity of sea surface fluctuations and random distributions. To address this issue, remote sensing methods based on SSR modulation have been used to study oceanographic phenomena. Sun glitter (SG), which is affected by SSR, is caused by the specular reflection of incident sunlight. Cox and Munk (1954) performed field experiments and developed a model (the CM model) to manifest the mathematical relationship between SG radiance and the SSR related wind-generated mean square of slope (MSS) using a symmetric slope probability density function (PDF), as well as the relationship between SSR and wind speed. This model laid the foundations for using SG images. Because SG depends primarily on SSR, it has been used as a crucial element for monitoring oceanic and limnological phenomena that affect SSR, such as internal waves (Apel et al., 1975; Jackson, 2007; Matthews and Awaji, 2010; Liu et al., 2014), underwater topography (Hennings et al., 1988; Hennings et al., 1994; He et al., 2014; Shao et al., 2014; Zhang et al., 2014), and oil slicks (Hu et al., 2009; Lu et al., 2016).

Subsequent studies used remote sensing techniques to investigate multi-angle SG. For example, Matthews (2005) used Advanced Spaceborne Thermal Emission and Reflection Radiometer (ASTER) stereo images to study internal waves, swell waves, bottom topography, and suspended sediment transport in nadir and backward-looking views. Similarly, the Multi-angle Imaging SpectroRadiometer (MISR) was found to be capable of discriminating oil spills and improving the operational monitoring of oil releases (Chust and Sagarminaga, 2007). Yang et al. (2015) presented multi-angle SG image characteristics of submarine sand waves in ASTER images. In addition, by adopting an iterative retrieval method to fit the wind speed by searching for the best

* Corresponding author.
E-mail address: zhanghg@sio.org.cn (H. Zhang).

https://doi.org/10.1016/j.rse.2018.02.004
Received 17 April 2017; Received in revised form 10 January 2018; Accepted 8 February 2018

linear correlation between the measured probability from multi-angle images and the model, Bréon and Henriot (2006) published their work of retrieving the wind from multi-angle (14 angles) images from the Polarization and Directionality of the Earth Reflectances (POLDER) instrument. Fox et al. (2007) explored the relationship between the MISR-observed width of the sun glint pattern over ocean waters and the near-surface wind speed, and these data were then used to develop an algorithm for wind retrieval. Harmel and Chami (2012) developed a scheme to directly retrieve the wind speed from a passive satellite sensor in the visible/near infrared bands (PARASOL) by an iteration process. With many view angles and a large region of hundreds of kilometers in width to calculate the width of the sun glint pattern over the ocean, the methods of Bréon and Henriot (2006) and Fox et al. (2007) can yield the wind speed of a large region, and entire images or sub-images can be obtained by an iteration process. However, these methods do not work for sensors with only two look angles, such as ASTER. Kudryavtsev et al. (2017a, 2017b) developed a practical method for quantitatively retrieving directional spectra of ocean surface waves from near-multidirectional SG imagery from the staggered detectors of the Copernicus Sentinel-2 Multi-Spectral Instrument. The ratio of sea surface slopes satisfies the conditions of specular reflections and MSS from the CM model proposed to evaluate the surface brightness modulation of capillary waves. However, given the limitations, it is still difficult to quantitatively extract SSR information, especially at a pixel scale.

Because of the short duration between multiple ASTER observations, the sea state, including SSR and wind speed, can be considered as nearly constant; therefore, multi-angle, even bi-angle, SG remote sensing images have potential for use in SSR estimations. In this study, we established a new estimation model for SSR by using multi-angle SG images. In addition, we performed a validation experiment for the estimated SSR with stereo optical images from the ASTER sensor. The estimation results were compared to reanalysis and buoy wind data to demonstrate that this model can be used to determine both the SSR of oceanographic features and the wind-generated background SSR related wind speed. Then, to illustrate the high-resolution SSR at a pixel scale, three oceanographic cases were introduced based on the estimated SSR data. Finally, the sensitivities of the atmospheric correction, view angle, and band wavelength were discussed.

2. Models

2.1. Model for multi-angle sun glitter remote sensing

Matthews (2005) discussed the geometry of SG observations in ASTER images associated with the nadir and back-looking views, but that study only considered one side of the nadir in the calculations even though the view angles may differ when the ASTER image is obtained from both sides of the nadir. Yang et al. (2015) improved the SG geometry model and considered the difference in the viewing angle among pixels in multi-angle images acquired by the ASTER sensor. As shown in Fig. 1, θ_0 and $\varnothing_0$ represent the sun zenith angle and the sun azimuth angle of each pixel, respectively, and these parameters can be determined by each pixel's position and imaging time. The symbols θ_N and $\varnothing_N$ denote the view angle and the sensor zenith angle in the nadir view image (NVI), respectively, and the view angle and the sensor zenith angle in the back-looking view image (BVI) are θ_B and $\varnothing_B$, respectively. These sensor angles can be determined by the scene orientation angle (S) and pointing angle (P) provided in the header file of ASTER images (Yang et al., 2015).

The SG radiance, L_g, after Gordon and Wang (1992) and Gordon (1997) was adopted in this study:

$$L_g = \frac{F_0 T_0 R(\omega)}{4cos\theta cos^4\beta} p(z_x, z_y), \tag{1}$$

where F_0 denotes the solar irradiance at the top of the atmosphere, T_0 denotes the downwelling direct transmittance, ω denotes the local reflection angle (Zeisse, 1995), θ denotes the view angle, β denotes the surface tilt angle of a facet on the sea surface, $R(\omega)$ denotes the Fresnel reflection coefficient, and $p(z_x, z_y)$ denotes the PDF of the wave slope as functions of individual slope components z_x and z_y. ω and β are computed from the sun and view zenith angle as well as the relative azimuth, which change from pixel to pixel.

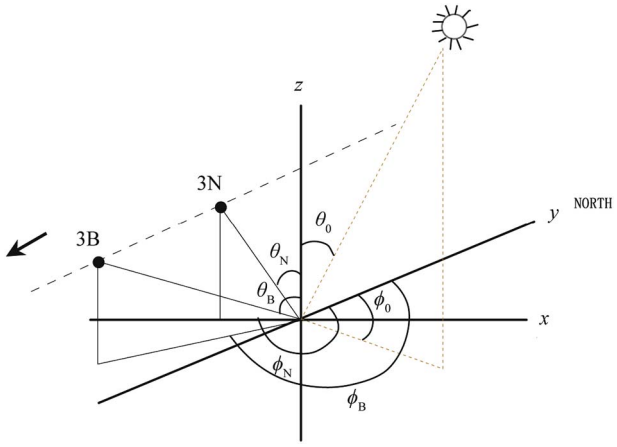

Fig. 1. Observational geometry of ASTER stereo-image pairs (after Yang et al. (2015)). Sun zenith angle (θ_0), nadir view angle (θ_N), backward-looking view angle (θ_B), sun azimuth angle ($\varnothing_0$), sensor azimuth angle in the nadir view ($\varnothing_N$), and sensor azimuth angle in the backward-looking view ($\varnothing_B$) are presented. The relative azimuth angles between the sun and sensor can be calculated by $\varnothing_0$, $\varnothing_N$, and $\varnothing_B$.

According to the CM model (Cox and Munk, 1954; Munk, 2009), the isotropic PDF without wind direction dependence was used, and it was determined as follows:

$$p(z_x, z_y) = p(\beta) = \frac{1}{\pi(\sigma_0^2)} \exp\left[-\frac{\tan^2\beta}{\sigma_0^2}\right], \tag{2}$$

where ${\sigma_0}^2$ denotes the wind-generated SSR. Zhang and Wang (2010) evaluated several empirical expressions of ${\sigma_0}^2$ as a function of wind speed in popular SG models and found that the CM model had the best performance. Therefore, the isotropic model was used in this study, and it can be presented as follows:

$$\sigma_0^2 = 0.003 + 0.00512U_0, \tag{3}$$

where U_0 denotes the wind speed (in $m\,s^{-1}$) 41 ft (12.5 m) above the sea surface.

By combining Eqs. (1) and (2), we get:

$$L_g = \frac{F_0 T_0 R(\omega)}{4\cos\theta\cos^4\beta} \frac{1}{\pi(\sigma_0^2)} \exp\left[-\frac{\tan^2\beta}{\sigma_0^2}\right]. \tag{4}$$

According to Eq. (4), the SG radiance is mainly determined by the image geometry angles and MSS (${\sigma_0}^2$).

2.2. Estimation model for sea surface roughness

Because of the very short duration between two ASTER observations, which amounts to an interval of approximately 55 s, the solar elevation angle and sun azimuth angle, as well as the sea state, can be considered almost unchanged, which means that SSR does not change significantly between observations. Therefore, according Eq. (4), the SG radiances of the two multi-angle SG images both follow:

$$L_{gN} = \frac{F_0 T_0 R(\omega_N)}{4\cos\theta_N\cos^4\beta_N} \frac{1}{\pi(\sigma_0^2)} \exp\left[-\frac{\tan^2\beta_N}{\sigma_0^2}\right] \tag{5}$$

and